JACS
JOURNAL OF THE AMERICAN CHEMICAL SOCIETY
Article
pubs.acs.org/JACS

Precision vs Flexibility in GPCR signaling

Matthias Elgeti,*[,†] Alexander S. Rose,[†] Franz J. Bartl,[†,‡] Peter W. Hildebrand,[†] Klaus-Peter Hofmann,*[,†,‡] and Martin Heck[†]

[†]Institut für Medizinische Physik und Biophysik (CC2), Charité-Universitätsmedizin Berlin, Charitéplatz 1, 10117 Berlin, Germany
[‡]Zentrum für Biophysik und Bioinformatik, Humboldt-Universität zu Berlin, Invalidenstrasse 42, 10115 Berlin, Germany

Supporting Information

ABSTRACT: The G protein coupled receptor (GPCR) rhodopsin activates the heterotrimeric G protein transducin (Gt) to transmit the light signal into retinal rod cells. The rhodopsin activity is virtually zero in the dark and jumps by more than one billion fold after photon capture. Such perfect switching implies both high fidelity and speed of rhodopsin/Gt coupling. We employed Fourier transform infrared (FTIR) spectroscopy and supporting all-atom molecular dynamics (MD) simulations to study the conformational diversity of rhodopsin in membrane environment and extend the static picture provided by the available crystal structures. The FTIR results show how the equilibria of inactive and active protein states of the receptor (so-called metarhodopsin states) are regulated by the highly conserved E(D)RY and $Yx_7K(R)$ motives. The MD data identify an intrinsically unstructured cytoplasmic loop region connecting transmembrane helices 5 and 6 (CL3) and show how each protein state is split into conformational substates. The C-termini of the Gtγ- and Gtα-subunits (GαCT and GγCT), prepared as synthetic peptides, are likely to bind sequentially and at different sites of the active receptor. The peptides have different effects on the receptor conformation. While GγCT stabilizes the active states but preserves CL3 flexibility, GαCT selectively stabilizes a single conformational substate with largely helical CL3, as it is found in crystal structures. Based on these results we propose a mechanism for the fast and precise signal transfer from rhodopsin to Gt, which assumes a stepwise and mutual reduction of their conformational space. The mechanism relies on conserved amino acids and may therefore underlie GPCR/G protein coupling in general.

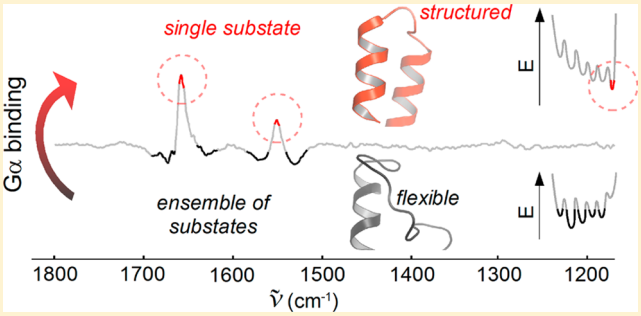

INTRODUCTION

G protein coupled receptors (GPCRs) receive signals from a variety of extracellular ligands and transmit them to intracellular G proteins. Ligands include activating agonists and deactivating inverse agonists. In their agonist-bound active state, GPCRs catalyze the exchange of GDP for GTP in the α-subunit of heterotrimeric G proteins.[1] In the GTP-bound active form, the G$\alpha\beta\gamma$ holoprotein dissociates and the Gα- and G$\beta\gamma$-subunits couple to intracellular effectors thereby triggering various signaling pathways. In the past decade crystal structures of several GPCRs were solved providing a molecular picture of different receptor states, including inactive conformations bound to inverse agonists and structures which are supposed to represent the active, G protein activating conformation.[2] These active structures exhibit gross structural changes compared to the inactive ones and bind agonistic ligands, G protein, fragments of the Gα-subunit or nanobodies (see ref 3). The major prerequisite of an active GPCR is an outward tilted transmembrane helix 6 (TM6) which was first identified by pioneering EPR work with the retinal photoreceptor rhodopsin,[4,5] an archetype of class A GPCRs. In contrast to other GPCRs, rhodopsin bears its light-sensitive ligand, retinal, covalently bound by a protonated Schiff base. The absorption of a photon induces 11-*cis*-/all-*trans*-retinal isomerization and switches the ligand from an inverse agonist to a potent agonist. The subsequent activating adjustments in the protein culminate in coupled equilibria between inactive and active states of the receptor, the so-called metarhodopsin states. Eventually, light-activated rhodopsin decays by hydrolysis of the Schiff base and dissociation of all-*trans*-retinal, leaving the opsin apoprotein. Opsin exhibits, like metarhodopsin, active and inactive states in equilibrium. Because the metarhodopsin and opsin states have structural equivalents in other GPCRs,[6,7] it can be concluded that rhodopsin shares, after the actual photoactivation phase, important properties with GPCRs binding diffusible ligands.

A key region for the coupling of rhodopsin with the G protein transducin (Gt) is the third cytoplasmic loop (CL3) connecting TM5 and TM6 and located adjacent to the conserved E(D)RY motif.[8−10] In the crystal structures of most GPCRs in their inactive conformation CL3 is a long protein segment with high flexibility, as indicated by high temperature factors or lack of electron density. Thus, in many GPCR structures CL3 is truncated or substituted by a fusion

Received: May 22, 2013
Published: July 24, 2013

   dx.doi.org/10.1021/ja405133k | J. Am. Chem. Soc. 2013, 135, 12305−12312

protein to minimize its flexibility.[11] In contrast, CL3 appears more structured in all crystal structures of active GPCRs with bound G protein (or mimicking fragments), even though in GPCRs exhibiting longer CL3, e.g., in the β_2-adrenergic receptor, it remains partially unresolved.[12,13] CL3 is therefore a strong candidate to represent an intrinsically disordered protein region. Such regions become ordered only upon binding to interacting partners and have high functional relevance for binding and regulation in various biological systems.[14] The question arises of how far the high flexibility of CL3 is exploited for G protein coupling, i.e., binding and activation.

In the present study we performed FTIR difference spectroscopy of the photoreceptor rhodopsin in the absence or presence of interacting peptide fragments of two G protein key binding sites (C-termini of Gtα and Gtγ). Using a novel titration approach we identify the binding modes of the two Gt fragments and provide support for the existence of different binding sites. Site-directed mutagenesis indicates a structural transition of CL3 which appears to be triggered by interaction with the C-terminus of Gtα (GαCT), while the C-terminus of Gtγ (GγCT) does not influence this region. All-atom molecular dynamics (MD) simulations using rhodopsin crystal structures as templates support the notion of high CL3 flexibility in all receptor states except when GαCT peptide is bound. We propose a mechanism of GPCR/G protein coupling employing two different interaction modes of rhodopsin with GαCT and GγCT peptide, respectively. In agreement with our previously proposed "sequential fit" model, the actual coupling with the Gt holoprotein would first employ interaction with the Gtγ subunit. This interaction directs the holoprotein such that the more specific interaction with Gtα can readily occur, eventually leading to the release of GDP and nucleotide exchange.

EXPERIMENTAL SECTION

FTIR Spectroscopy. Rhodopsin in washed membranes was prepared from frozen bovine retinae (W.L. Lawson Company, U.S.A.) using a protocol similar to ref 15. Membrane pellets were obtained after pH adjustment by centrifugation at 10 000 *g*, Gt-derived peptides (GαCT 340-350, IKENLKDCGLF and GαCT2 340-350, ILENLKDCGLF synthesized by Selleck chemical, and farnesylated GγCT 60-71, DKNPFKELKGGC-far and nonbinding GγCT 60-71, DKNPAKEAKGGC-far,[16] synthesized by Dr. Petra Henklein, Institut für Biochemie, Charité, Berlin) were added before centrifugation. K231A mutant and wild-type (WT) receptor reconstituted in lipid vesicles were prepared as described.[17] Time-dependent FTIR difference spectra were recorded on an ifs66v/s FTIR spectrometer (Bruker, Ettlingen, Germany) equipped with a MCT detector. Raw data were processed in self-written MATLAB routines comprising baseline correction, singular value decomposition, matrix rotation, and global fitting.[18] See the SI Methods section for in-depth description of the spectroscopic and analytic techniques.

MD Simulations. Three different models were prepared based on the crystal structures of rhodopsin dark state (pdb 1U19) and the opsin/GαCT complex (3DQB). Rhodopsin dark state serves as reference of an inactive GPCR, while active opsin contains all gross structural features of the active conformation, e.g., the prominent outward tilt of TM6.[19] The palmitoylated receptors were equilibrated in a DMPC lipid bilayer, and three 200−400 ns nonbiased all-atom MD simulations were performed, each set starting from the same initial model. Subsequent cluster analysis regarding the residues 224−252 from CL3 was performed with a 2 Å root-mean-square deviation (RMSD). Further information on *in silico* preparation, simulation protocols, and cluster analysis is found in the SI.

RESULTS

Conformational Diversity of the Agonist-Bound Receptor. In the following we use the three step equilibrium scheme of metarhodopsin states to describe the diversity of agonist-bound receptor conformations. These equilibria are reached within milliseconds after illumination of dark state rhodopsin in native membranes, with a distribution that strongly depends on pH and temperature.[20]

Previous work has shown that the metarhodopsin states exhibit distinct FTIR characteristics. For formation of metarhodopsin I (MI), infrared spectroscopy using azido probes[21] has revealed only slight rearrangements of the 7TM bundle with respect to dark-state rhodopsin. The subsequent formation of MIIa involves deprotonation of the retinal Schiff base linkage and formation of a new hydrogen bond of the carboxyl side chain of D83$^{2.50}$ (Ballesteros-Weinstein numbering, transmembrane residues are assigned two numbers X.Y, where X is the belonging helix and Y the number relative to the most conserved residue in this TM, which is assigned 50. We use H8 or CL3 for residues of helix 8 and third cytoplasmic loop, respectively) located in the Schiff base vicinity. This is reflected by an arising FTIR difference band at 1768/1752 cm^{-1}, meaning that the vibration shifts from 1768 cm^{-1} (dark state) to 1752 cm^{-1} in MIIa.[22] MIIb formation is accompanied by large difference bands in the amide I (∼1650 cm^{-1}) and amide II (∼1550 cm^{-1}) regions and at 1745/1727 cm^{-1}. The latter mirrors the reorganization of the important TM3/TM5 hydrogen-bond network involving the side chain of E122$^{3.37}$.[23] This difference band marks the rotational outward tilt of TM6, which is a prerequisite of a G protein activating receptor conformation. The subsequent formation of MIIbH$^+$ is "spectroscopically silent", i.e., not coupled to conformational changes large enough to give rise to distinct FTIR bands.[20]

Figure 1A shows FTIR difference spectra, each recorded at a different pH value between 5 and 9.3. The pH-dependent intensity changes of the two FTIR difference bands at 1768/

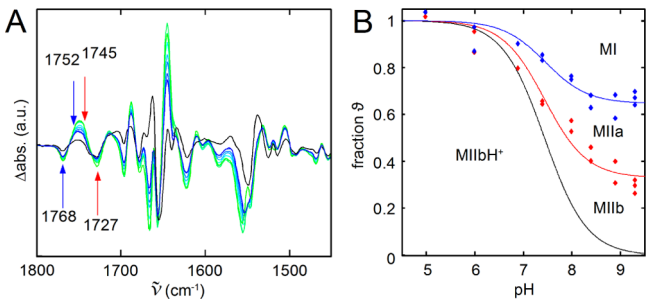

Figure 1. FTIR spectroscopic characterization of metarhodopsin states. (A) FTIR difference spectra of rhodopsin in disk membranes (photoproduct minus dark state) measured at 30 °C and in the range of pH 5.0 (light-green spectrum) to pH 9.3 (blue spectrum). The black spectrum was obtained under conditions favoring formation of MI (pH 8.5, −14 °C). Arrows indicate wavenumbers analyzed in (B). (B) pH dependence of the FTIR difference bands at 1768/1752 (blue) and 1745/1727 cm^{-1} (red) calculated from the spectra shown in (A). The data points represent the difference between the respective difference spectra and the MI difference spectrum and are normalized to the maximum difference obtained between the MI reference and pH 5.5. Lines show best fits of the data points to a modified Henderson−Hasselbalch equation, the black curve was calculated using Scheme 1. See text for the assignment of titration curves to the respective fractions of the metarhodopsin states (MI, MIIa, MIIb, and MIIHb+).

dx.doi.org/10.1021/ja405133k | J. Am. Chem. Soc. 2013, 135, 12305−12312

1752 cm^{-1} (blue) and 1745/1727 cm^{-1} (red) are shown in Figure 1B, reflecting a population shift within the coupled equilibria (Scheme 1). These two titration curves were analyzed

Scheme 1

$$MI \rightleftharpoons MIIa \rightleftharpoons MIIb \rightleftharpoons MIIbH^+$$

using Scheme 1 yielding the fractions ϑ of the individual metarhodopsin states (see ref 20 and SI Methods 1.3). At high pH and 30 °C we find MI, MIIa, and MIIb significantly populated, each state to approximately one-third. All titration curves converge at low pH with an apparent pK_a of 7.5 indicating the selective stabilization of only one receptor state, $MIIbH^+$. This stabilization by proton uptake is further corroborated by temperature-dependent measurements at high and low pH, respectively (Figure S1).

Protein States That Interact with C-Terminal Fragments of the G Protein. To uncover which of the metarhodopsin states interact with GαCT and/or GγCT, we extended the above spectroscopic titration assay to samples in which peptides (P) of either binding region were present. Using Scheme 2 with the respective equilibrium constants K_{1-3} and

Scheme 2

$$\begin{array}{ccccc} MI & \overset{K_1}{\rightleftharpoons} & MIIb & \overset{K_2(pKa)}{\rightleftharpoons} & MIIbH^+ \\ & & K_3 \downuparrows & & \downuparrows\ a\cdot K_3 \\ & & MIIb\cdot P & \overset{a\cdot K_2}{\rightleftharpoons} & MIIbH^+\cdot P \end{array}$$

the parameter a representing the ratio between the peptide binding affinities of MIIb and $MIIbH^+$, the pH-dependent distribution of all species can be described.

We omit MIIa, as both MI and MIIa share a similar cytoplasmic conformation and the amount of MIIa is negligibly small under the experimental conditions (20 °C).[20] A fit of the pH dependent 1745/1727 cm^{-1} difference band (see SI Methods) yields the fraction of MI (inactive cytoplasmic surface), MIIb (TM6 outward tilted but $E134^{3.49}$ deprotonated), and $MIIbH^+$ (TM6 outward, $E134^{3.49}$ protonated). The resulting plot is shown in Figure 2A for a sample of native washed membranes in the absence of any peptide (i.e., when the amount of complexed species is zero). Consistent with Figure S1, the fit yielded a ratio of ca. 70/30 for MI to MIIb at

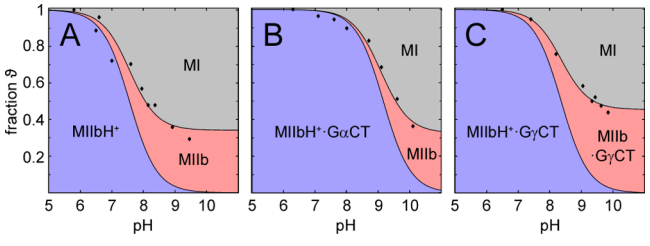

Figure 2. Effect of GαCT and GγCT peptides on the pH-dependent equilibrium of the metarhodopsin states. The pH dependencies of the relative fractions of MI (gray), MIIb (red), and MIIbH+ (blue) were calculated from FTIR difference spectra obtained at 20 °C: (A) in the absence of peptide, (B) in the presence of 10 mM GαCT, and (C) 10 mM GγCT, respectively. Data points are from the FTIR difference band at 1745/1727 cm^{-1} as described in Figure 1B, and the fractions of the metarhodopsin states are from numerical fits of the data points to a set of equations derived from Scheme 2.

the alkaline end point and a microscopic $pK_a = -\log(K_2)$ of 8.1 for proton uptake and formation of $MIIbH^+$.

Addition of 10 mM GαCT peptide changed the titration behavior of most difference bands. We found a selective stabilization of the protonated complexed species over the broad pH range from 5 to 9 (Figure 2B). Accordingly, the fit to the data yielded a dissociation constant $K_D = a\cdot K_3 = (330 \pm 80)$ μM ($a = 1.2 \times 10^{-4}$, $K_3 = 2.7$ M), which fits well to the value previously obtained with micromolar rhodopsin.[24] While the microscopic pK_a value remained unaffected, the apparent pK_a shifted to 9.1 in the presence of 10 mM peptide. Increasing the GαCT peptide concentration led to a further shift of the apparent pK_a, confirming our notion of a selective $MIIbH^+$ stabilization (see Figure S2).

Farnesylated GγCT peptide was also tested for its effect on the distribution of the metarhodopsin states. GγCT peptide (Figure 2C) had a different influence as compared to GαCT peptide. Besides a shift of the apparent pK_a to higher values, an increase of the alkaline end point level was also observed, meaning that MIIb is stabilized at the expense of MI. Consistently, the increase of peptide concentration led, as in the case of GαCT, to a more pronounced pK_a shift but also to a further elevation of the alkaline titration level (see Figure S3).

Effect of Peptide Binding on Receptor Structure. Peptide binding was further investigated through a so-called peptide binding spectrum (PBS), which is the difference between two difference spectra measured in the presence and absence of peptide (see Figure S5). Since all vibrational changes of the free receptor protein are subtracted from the difference spectrum of the receptor/peptide complex, the resulting PBS is a specific measure of peptide induced conformational changes in both receptor and peptide.[25−27]

In Figure 3 the peptide binding spectra of GαCT (A) and GγCT (B) peptide binding to the protonated $MIIbH^+$ state are

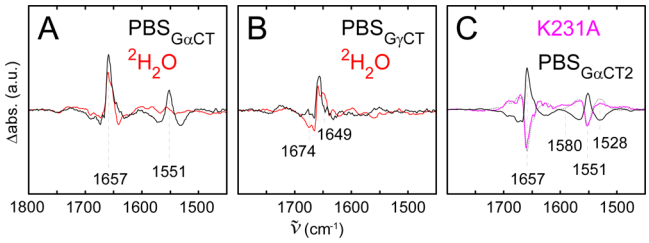

Figure 3. FTIR spectroscopic characterization of rhodopsin/peptide complexes and rhodopsin mutation K231A. Peptide binding spectra (PBS, black) of (A) 10 mM GαCT and (B) 10 mM GγCT, respectively. The red spectra are obtained after $H_2O/^2H_2O$ exchange under otherwise identical conditions (30 °C and pH 5.5). (C) FTIR double difference spectrum of rhodopsin mutant K231A mutant (magenta) and $PBS_{G\alpha CT2}$ (black) both obtained in lipid vesicles under conditions of $MIIbH^+$ formation (30 °C and pH 5). Note that the K231A-WT spectrum is scaled by a factor of 2 and $PBS_{G\alpha CT2}$ by a factor of 0.5. The inverted $PBS_{G\alpha CT2}$ is superimposed for better comparison (dotted gray line). Marked frequencies are discussed in the text, the respective difference spectra are shown in Figure S5.

shown. The PBS of GαCT peptide ($PBS_{G\alpha CT}$) is much more intense than that of GγCT peptide ($PBS_{G\gamma CT}$), especially in the structurally sensitive amide II region (1580−1540 cm^{-1}). This indicates that binding of GαCT has a greater influence on the structures of receptor and peptide than binding of GγCT, which causes mainly one positive difference band at 1657 cm^{-1}. The GγCT experiment was also performed with a nonbinding

dx.doi.org/10.1021/ja405133k | J. Am. Chem. Soc. 2013, 135, 12305−12312

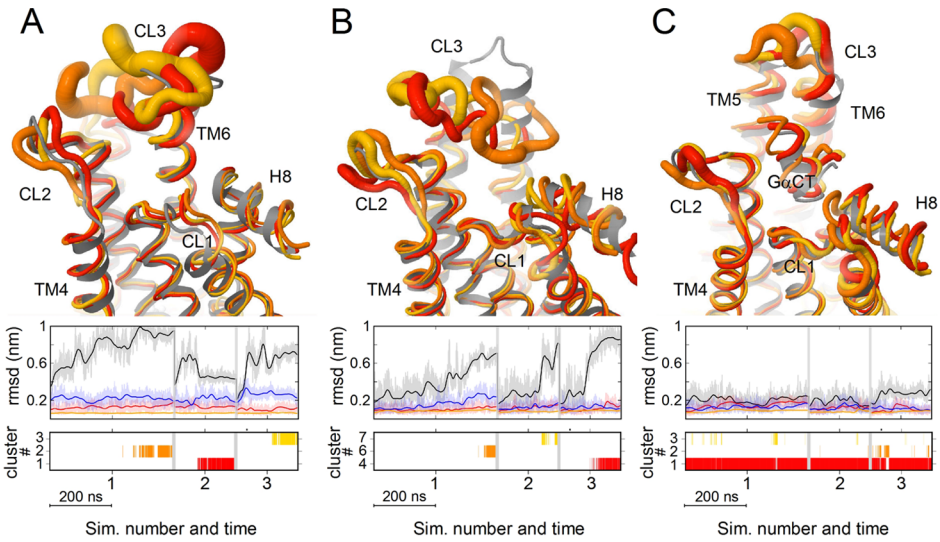

Figure 4. Conformational flexibility of CL3 analyzed by MD simulations. (A) Inactive, (B) active, and (C) active rhodopsin in complex with GαCT. Top row shows for each system the respective X-ray structure (gray) and three representative conformations (red, orange, yellow) obtained by cluster analysis. The tube thickness relates to fluctuations of each residue (RMSF) within a given cluster. The middle row depicts the RMSD for the transmembrane helices (orange), CL1 (red), CL2 (blue), and CL3 (black). The occurrences of depicted cluster conformations are given in the bottom row. (A) Three most occupied conformations (clusters 1−3) are shown indicating a highly flexible CL3. (B) Three metastable conformations are depicted (clusters 4, 6 and 7), which are adopted after leaving the initial conformation given by the X-ray structure. It is seen that these conformations vary significantly among each other and with respect to the starting structure. (C) The three most occupied conformations (clusters 1−3) are very similar to the initial conformation taken from the crystal structure. See Figure S6 for the full cluster analysis.

GγCT peptide variant. The respective PBS reveals that the control peptide had no influence on the difference spectrum (Figure S5), providing evidence for a specific interaction of the GγCT peptide with the active receptor. To gain insight into the specific molecular changes underlying $PBS_{G\alpha CT}$ and $PBS_{G\gamma CT}$, we performed corresponding experiments after $H_2O/^2H_2O$ exchange. The exchange causes distinct spectral shifts of molecular vibrations coupled to protonation and thus facilitates assignment of FTIR difference bands to their molecular origin, e.g., specific amino acids of backbone vibrations. As an example, the most likely candidate for parts of the 1657 cm^{-1} vibration is the guanidinium side chain of $R135^{3.50}$. $R135^{3.50}$ is known to be involved in GαCT binding,[10,28] and its frequency strongly depends on whether it is bound via salt bridge or hydrogen bond. Furthermore, the arginine $CN_3H_5^+$ vibration decouples after $H/^2H$ exchange, leading to a pronounced downshift and overall smaller difference bands in the 1650 cm^{-1} region. The remaining intensity changes are most likely amide I vibrations indicative of changes in the peptide backbone (e.g., secondary structure), as amide I bands are known to exhibit only small if any isotope shifts. Interestingly, the negative amide I and II bands are broadly distributed, while only one positive band arises in both regions. The position of the positive amide I band fits to the absorption of a solvent exposed α-helix. This suggests a structural transition from an unstructured to a clearly structured segment. The notion is further substantiated by the disappearing amide II vibrations of $PBS_{G\alpha CT}$ in ^2H_2O. Amide II bands can be utilized to probe the flexibility of protein regions, as amide protons undergo fast $H^+/^2H^+$ exchange in unstructured loops, while hydrogen bonds in structured regions are more protected even in solvent exposed protein parts (for a comprehensive review of FTIR signatures in proteins see ref 29). To estimate the number of amino acids involved in the structuring transition, we evaluated the GαCT binding induced absorbance change at 1657 cm^{-1} (in ^2H_2O to avoid the signal caused by nonamide I groups). Using $\varepsilon_{\text{amide I}} \approx 500\ M^{-1}\ cm^{-1}$,[30] we obtain five amino acids per rhodopsin molecule. However, this certainly underestimates the effect, as α-helix and random coil exhibit very similar amide I frequencies, and thus several positive and negative bands may overlap or even compensate each other.

The lack of pronounced amide II features in the $PBS_{G\gamma CT}$ (Figure 3B) excludes a significant influence of GγCT peptide binding on receptor structure as found for GαCT. The differences between the two peptides were further confirmed after ^2H_2O exchange, which led to a slightly more intense negative and an additional positive band in $PBS_{G\gamma CT}$, likely due to a shift of a positive band around 1674 to 1649 cm^{-1}. This fits to the absorption of a ν(C═O) vibration of glutamine or asparagine side chains involved in the binding process.

Effect of Single Site Mutation on the Structuring of CL3. $K231^{CL3}$ (the position of K231 depends on the respective crystal structure, either 5.66 or CL3, and as a result of our analysis, we use the notation $K231^{CL3}$) is part of the conserved $Y^{5.58}x_7K(R)^{CL3}$ motif located in CL3 and participates in a hydrogen-bond network consisting of $K231^{CL3}$, $E247^{6.30}$, and $T251^{6.34}$, which has been suggested to constitute a determinant of the active conformation[7] (see Figure S4). Consistently, biased MD simulations found a strong influence of the K231A mutation on the distribution of activated receptor conformations.[31] We therefore expressed the K231A mutant and reconstituted the mutant and the WT receptor protein separately into lipid vesicles as described.[17] Difference spectra were recorded under conditions which favor $E134^{3.49}$ protonation ($MIIbH^+$), and the corresponding double difference K231A minus WT was calculated to elucidate the structural consequences of the K231A mutation (Figure 3C). The double difference spectrum of K231A shares distinct similarities with $PBS_{G\alpha CT2}$, the peptide binding spectrum recorded for WT rhodopsin in lipid vesicles, but is inverted. This correlation suggests that the receptor conformation, which is stabilized by GαCT peptide binding, is also present to a small

dx.doi.org/10.1021/ja405133k | J. Am. Chem. Soc. 2013, 135, 12305−12312

but significant extent in the absence of GαCT peptide and that mutation of $K231^{CL3}$ destabilizes this conformation. The small residual differences between the K231A double difference and $PBS_{G\alpha CT2}$ have two molecular origins: Some are a direct consequence of the disrupted hydrogen-bond network in the K231A mutant (lysine, glutamate, or threonine vibrations cause absorptions around 1650 cm^{-1}), while others can be attributed to the structural changes of the GαCT2 peptide which account for parts of the $PBS_{G\alpha CT2}$ (e.g., at 1580 and 1528 cm^{-1}).[27]

MD Simulation of Receptor States. To specify the effect of GαCT on the CL3 structure, we performed several 200−400 ns classical all-atom MD simulations of membrane embedded rhodopsin starting from the crystal structures of the inactive[32] and the active[10] states with or without GαCT peptide. Comparison of the RMSD in the inactive and active states indicates that CL3 is more flexible than the other two cytoplasmic loops (Figure 4). To identify conformations of CL3 which were frequently occupied during the simulations, we performed a cluster analysis with respect to residues 224−251 (Figure S6). For each set of simulations three representative CL3 conformations and their occurrence during the simulations were used to monitor the structural heterogeneity of CL3 in the different underlying receptor states (Figure 4).

For dark-state rhodopsin the simulations suggest high CL3 flexibility (Figure 4A), which is in accordance with the high B-factors found in several of the crystal structures (e.g., pdb 1U19, see Figure S8). However, the distinct helical extension of TM6 into the aqueous phase seen in the crystal structure is preserved during all three simulations. For the active state in the absence of GαCT, the initial structured conformation of CL3 becomes disordered and highly flexible after <200 ns (Figure 4B). Among the different bent helical and coiled structures adopted, each is populated for <10% of the simulation period, with lifetimes of $\sim 10^{-8}$ s (as estimated from the timelines in Figure S6).

During the simulations of the receptor/GαCT complex, CL3 is rigid, and its secondary structure is preserved (Figure 4C). Nearly 95% of the CL3 conformations fall into the largest cluster (Figure S6C) which fluctuate around the α-helical rich CL3 conformation found in the crystal structure (Figure 4C, gray). The flexibility changes of CL3 were dissected on the level of individual amino acids by calculating their root-mean-square fluctuations (RMSF). Receptor activation results in a loss of flexibility specifically around A233, while the region around K248 becomes more flexible. Notably, binding of GαCT peptide constrains all residues within CL3 (Figure S7). The salient result of the simulations is therefore that CL3 is likely to be intrinsically disordered, becoming structured and more rigid upon binding of GαCT.

Crystal Contacts in Available GPCR Structures. To evaluate the possible influences of crystallization on the secondary structure of CL3, we analyzed the available crystal structures of GPCRs with respect to the CL3 conformations (Table S1). Structures where CL3 had been truncated or fusioned to a soluble protein were excluded. We find a shorter CL3 in the presence of cytoplasmic binding partners, such as G protein, GαCT peptides, or G protein mimetic nanobody. There is also a strong correlation between specific crystal contacts within CL3 and its secondary structure. Particularly, these crystal contacts stabilize elongated helices TM5 or TM6 at the cost of CL3. This is especially important to note for the rhodopsin case, where all structures representing active conformations exhibit crystal contacts between CL3 and TM1/H8 of the adjacent receptor molecule (Figure S8B). The structuring of CL3 may thus be artificial in these crystal structures and CL3 actually more flexible in the underlying protein states.

DISCUSSION

In this study, we employed FTIR spectroscopy and MD simulations of rhodopsin in the membrane environment to extend the static picture from X-ray analysis by complementary dynamic information. To classify the information, we will follow the hierarchical concept of protein dynamics developed by Frauenfelder and co-workers.[33] The concept distinguishes three classes of conformational states by their different lifetimes. We will identify several receptor conformations as protein states (tier 0), which exhibit a lifetime greater than a microsecond. Each protein state comprises several taxonomic substates (tier 1) with nanosecond lifetimes. These taxonomic states can be further subdivided into so-called statistical substates (tier 2), which form and decay on the picosecond time scale, respectively.[34] The interpretation of our results is based on the notion that transitions between protein states are facilitated by transitions between taxonomic substates.[35] Finally, this led us propose a model of how signal transfer from an activated receptor molecule to the G protein may occur.

Proton Uptake Reduces the Conformational Diversity of Receptor States and Leads to a Tightening of the GαCT Binding Cleft. The conformational diversity of light-activated rhodopsin is reflected in the scheme of metarhodopsin (M) states. We assign these states to protein states (tier 0) as they form and decay on the microsecond to millisecond time scale (Figure 5A, see ref 7 for review). Notably, all metarhodopsin states are populated to a significant amount

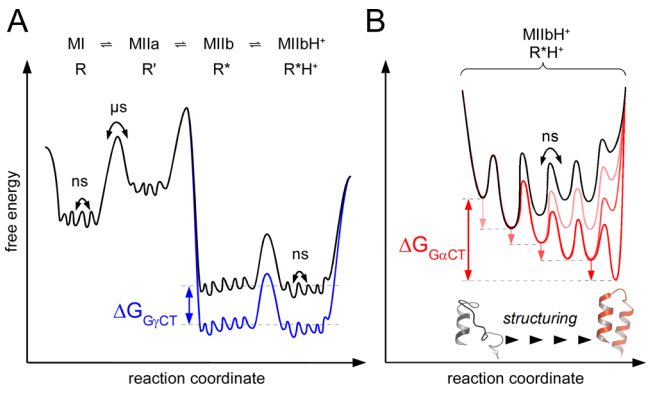

Figure 5. Energy landscape of the agonist bound receptor states. (A) Schematic free energy landscape illustrating the change of receptor conformations along the thermal activation path under physiological conditions. Each metarhodopsin state (or the corresponding generalized receptor state R of other GPCRs) has a lifetime exceeding microseconds and comprises several taxonomic substates with nanosecond lifetimes. GγCT binds to both MIIb (R*) and $MIIbH^+$ (R^*H^+) with similar affinities, i.e., equally stabilizes both receptor states by lowering their free energy (blue line). (B) GαCT specifically binds to the protonated active receptor state ($MIIbH^+$, R^*H^+), thereby stabilizing a single taxonomic substate. Upon binding of GαCT the initially unstructured CL3 (gray cartoon, structure taken from dark state, pdb 1U19) is stepwise adjusted and eventually adopts the conformation found in the crystal structure of active, GαCT peptide bound opsin (red cartoon, pdb structure taken from 3DQB). Note that the individual energy levels and energy barriers are only schematic and do not represent experimentally obtained values.

dx.doi.org/10.1021/ja405133k | J. Am. Chem. Soc. 2013, 135, 12305−12312

under physiological conditions (at least 10% each).[22] It was conceived early on that metarhodopsin states correspond to structurally equivalent inactive (R) and active (R*) states of other GPCRs.[36] Because the outward tilt of TM6, the structural prerequisite of GPCR activation, occurs with formation of MIIb,[4,37] we correlate this state with the active R* state and accordingly the protonated state MIIbH$^+$ with R*H$^+$ (Figure 5A). A similar assignment has been more recently suggested by Deupi and Kobilka.[6]

In agreement with earlier studies we found that three deprotonated protein states, namely R, R′, and R* coexist at high pH (see Figure 1B), all containing the intact salt bridge between E134$^{3.49}$ and R135$^{3.50}$.[20,22] However, proton uptake at low pH leads to disruption of the E134$^{3.49}$–R135$^{3.50}$ ionic interaction and stabilization of the protonated active state R*H$^+$. The important question arises, which global structural changes are coupled to the proton uptake that is mandatory for full catalytic activity of the receptor.[38] In the structures of the inactive receptor, TM5 is kinked with highly conserved Pro215$^{5.50}$ serving as a hinge, while in the active receptor TM5 appears fully elongated with a slightly inwardly translated cytoplasmic end (see Figures S4 and S8). Recently, we could show that inward stabilization of TM5 occurs only upon proton uptake.[17] We hypothesize that, in its inward position, TM5 constitutes a "doorstop", hindering TM6 to leave its active outward tilted conformation. Furthermore we propose that the inward position of TM5 leads to a tightening of the cleft between TM3, TM5, and TM6 which constitutes the binding site of the C-terminus of the G protein α-subunit. Consistently, the MD analysis of CL3 flexibility suggests a stabilization of the cytoplasmic end of TM5 upon formation of R*H$^+$ (Figure S7). The proposed doorstop mechanism is a possible explanation of how the uptake of a single proton suffices to reduce the conformational diversity to only one protein state.

Binding of GαCT Peptide Stabilizes Only One Conformational Substate of the Protonated Active Receptor. NMR spectroscopic studies have shown that the key binding fragment of Gt, the extreme C-terminus of the Gα subunit (GαCT peptide), forms an α-helix upon binding to the photoactivated receptor.[39] Furthermore, FTIR spectroscopy has shown that GαCT binding also affects the receptor structure.[27] However, the influence of peptide binding on the receptor structure is in apparent contradiction to X-ray crystallography, since the receptor with or without GαCT peptide does not exhibit substantial conformational differences.[10,28,40] Analyzing a large set of GPCR structures, we found that this structured CL3 conformation is stabilized not only by GαCT or other stabilizing agents but also by crystal contacts (Table S1), which explains the great similarity of active rhodopsin/opsin structures with or without GαCT peptide. Accordingly, our MD simulations suggest that the active receptor conformation in the absence of GαCT peptide comprises different bent and helical conformations of CL3, while the other cytoplasmic loops and helix 8 are considerably less flexible (Figure 4B). The different CL3 conformations exhibit lifetimes in the range of 10^{-8} s, which suggests that these conformations are taxonomic substates of R*H$^+$ (tier 1, Figure 5B). Our findings are in agreement with results obtained by an elaborate EPR analysis of the structural features of CL3.[41] The broadly distributed negative FTIR features are compatible with the finding from MD simulations, suggesting that CL3 is disordered and exhibits many different substate conformations in the GαCT unbound state. Furthermore, both our spectroscopic and *in silico* results point to the fact that GαCT peptide stabilizes one specific taxonomic substate of R*H$^+$ that exhibits a largely helical conformation of CL3. That CL3 constitutes an intrinsically unstructured protein domain which becomes structured upon complex formation has been already suggested on the basis of sequence analysis.[42]

Prior to their coupling, CL3 as well as GαCT are disordered,[39,43] and coupling of these two domains would become extremely slow when a pure conformational selection of the structured substates is assumed. Based on the data obtained in this study, we therefore propose a sequential binding mechanism comprising several steps of conformational selection and induced fit: In the first step, the long-range charge potential of R135$^{3.50}$ ($\sim 1/r$) is likely to support formation of an encounter complex[44] between activated receptor and GαCT. The subsequent forced proton uptake of the receptor would then lead to the inward "doorstop" movement of TM5 and thus contraction of the binding site. Such a GαCT induced tightening of the receptor binding domain has already been suggested on the basis of radiolytic footprinting data.[45] At this stage of the reaction, we hypothesize that short-range hydrophobic interactions ($\sim 1/r^6$) can build up. The associated expulsion of water molecules would then promote helix formation in both GαCT and CL3. The proposed mechanism of stepwise complex formation includes several stages of mutual adjustment[46] each accompanied by a population shift of taxonomic substates along the reaction coordinate. This corresponds to a progressively altered energy landscape (Figure 5B), such that in each individual step, the next, more specific conformation along the binding trajectory is selected. Within the resulting binding funnel,[47] multiple taxonomic substates are transiently populated, each contributing merely a nanosecond lifetime.

GγCT Binds to Both the Protonated and Deprotonated Active Receptor. The crystal structure of the β_2-adrenergic receptor in complex with the Gs holoprotein[12] does not show any interaction of GγCT with the receptor. However, GγCT peptide does specifically interact with light-activated rhodopsin, i.e., stabilize MII conformations at the expense of MI.[24] The present titration assay now demonstrates that GγCT peptide (in contrast to GαCT peptide) interacts with both MIIb (R*) and MIIbH$^+$ (R*H$^+$) with similar affinities (Figure 5A). This means that the interaction with GγCT peptide does not distinguish whether the E134$^{3.49}$–R135$^{3.50}$ salt bridge is intact or broken or whether TM5 is in- or outward tilted, which is also consistent with the finding that GγCT binding does not lead to structuring of the CL3 region (Figure 3).

In light of these observations, we assume that GγCT occupies a binding site different from GαCT. Because GαCT and GγCT peptides have been shown to compete with one another for binding to the active receptor,[48] the GγCT binding site is likely to be allosterically coupled to the GαCT binding cleft. Such allostery has to span the ∼40 Å distance between the Gα and Gγ C-termini in the footprint of the Gt holoprotein.[43] The most distant region from the rim of CL3 is the end of cytoplasmic helix 8 (43 Å between Cα-atoms of Q238^{CL3} and Cys323^{H8} in the crystal structure of active opsin). This region has already been suggested to interact with the Gt holoprotein[49] and is coupled to the ERY motif via the highly conserved residues of the NPxxYx$_{5/6}$F motif.[50] Monomeric rhodopsin thus provides a possible structural basis for an allosteric mechanism, in agreement with the finding that rhodopsin monomers efficiently activate Gt.[51,52] However, we

cannot exclude that the Gα and Gγ C-termini can also bind to different protomers within a receptor dimer.[53]

Mechanistic Implications for GPCR-Mediated Signal Transduction. Rhodopsin's perfect switching function depends on two factors: signal fidelity and speed. Fidelity relies in the first instance on the inactivating and activating retinal ligands which are covalently bound to the receptor and sufficiently potent to shift the equilibria of receptor conformations to the inactive or active side. Equally important, however, is an accurate and productive coupling mechanism of the activated receptor and G protein (up to more than 10^3 G proteins per second).[54] To tackle the latter point, we now specify our previously proposed "sequential fit" model of rhodopsin/transducin coupling[24,48,55] by structural and dynamic details obtained from FTIR spectroscopy and MD simulations.

Upon receptor activation the first specific contact is likely to occur between receptor and the Gγ C-terminus. On the one hand GγCT exhibits a lipid anchor which is likely to ensure more efficient collisional coupling by reducing the G protein diffusion to a two-dimensional space. On the other hand our results show that binding of GγCT to the active receptor is less selective than binding of GαCT, as GγCT peptide is capable of interacting with any active receptor form irrespective of the receptor's protonation state (Figure 5A). According to this scenario, the initial receptor−GγCT interaction would confine the search of the Gα C-terminus for its specific binding site to a one-dimensional rotational space. The intrinsically unstructured nature of CL3 maximizes its capture radius and thus accelerates the encounter with the C-terminus of the Gα-subunit.[56] Hence, the subsequent mutual structuring steps of receptor and GαCT are nothing but a population shift of taxonomic substates (of R^*H^+) proceeding on the nanosecond time scale (Figure 5B). Accordingly, a decrease of Gα C-terminal flexibility between initial GDP-bound and final GDP-free receptor/G protein complex was identified in HD exchange measurements of interaction between β_2-adrenergic receptor and Gsαβγ.[57] We therefore assume that the fully structured binding site found in the crystal structure of the rhodopsin/GαCT complex correlates to the empty site state after GDP release. Taken together, the tight complex provides the large and stable interaction surface required for the precise interrogation of structural elements to realize high signal fidelity.

Thermodynamically, the formation of a specific secondary structure with minimized degrees of conformational freedom constitutes an entropic cost. This needs to be counterbalanced by the energy gain of new bonds, hydrophobic contacts, or dehydration and possibly by an increased flexibility in other parts of the G protein.[58] In any case, the intrinsic propensity to unfold opens the possibility of rapid dissociation after signal transfer. The balance between enthalpic and entropic driving forces is implemented in the precision and flexibility of GPCR and G protein key binding sites to build a functional catalytic module.

■ ASSOCIATED CONTENT

Supporting Information

Further information on sample preparation, data analysis, and MD simulation protocols. This material is available free of charge via the Internet at http://pubs.acs.org.

■ AUTHOR INFORMATION

Corresponding Author

matthias.elgeti@charite.de; klaus_peter.hofmann@charite.de

Notes

The authors declare no competing financial interest.

■ ACKNOWLEDGMENTS

We are grateful to Jana Engelmann, Anja Koch, and Brian Bauer for expert technical assistance, Roman Kazmin for the preparation of the K231A and WT in lipid vesicles, and Friedrich Siebert for assistance with the interpretation of the FTIR data. We thank Helmut Grubmüller and Ulrich Zachariae for providing additional computing resources and assistance with running the MD simulations. The computer time necessary for this project was provided by the "Norddeutscher Verbund für Hoch- und Höchstleistungsrechner" (HLRN). This work was funded by the Deutsche Forschungsgesellschaft (SFB 740 to K.P.H., P.W.H., and M.H.) and the European Research Council (TUDOR to K.P.H).

■ REFERENCES

(1) Hepler, J. R.; Gilman, A. G. *Trends Biochem. Sci.* **1992**, *17*, 383−7.
(2) Rosenbaum, D. M.; Rasmussen, S. G. F.; Kobilka, B. K. *Nature* **2009**, *459*, 356−63.
(3) Katritch, V.; Cherezov, V.; Stevens, R. C. *Trends Pharmacol. Sci.* **2012**, *33*, 17−27.
(4) Farrens, D. L.; Altenbach, C.; Yang, K.; Hubbell, W. L.; Khorana, H. G. *Science* **1996**, *274*, 768−70.
(5) Altenbach, C.; Kusnetzow, A. K.; Ernst, O. P.; Hofmann, K. P.; Hubbell, W. L. *Proc. Natl. Acad. Sci. U.S.A.* **2008**, *105*, 7439−44.
(6) Deupi, X.; Kobilka, B. K. *Physiology* **2010**, *25*, 293−303.
(7) Hofmann, K. P.; Scheerer, P.; Hildebrand, P. W.; Choe, H.-W.; Park, J. H.; Heck, M.; Ernst, O. P. *Trends Biochem. Sci.* **2009**, *34*, 540−52.
(8) Franke, R. R.; Konig, B.; Sakmar, T. P.; Khorana, H. G.; Hofmann, K. P.; König, B. *Science* **1990**, *250*, 123−5.
(9) Ernst, O. P.; Hofmann, K. P.; Sakmar, T. P. *J. Biol. Chem.* **1995**, *270*, 10580−6.
(10) Scheerer, P.; Park, J. H.; Hildebrand, P. W.; Kim, Y. J.; Krauss, N.; Choe, H.-W.; Hofmann, K. P.; Ernst, O. P. *Nature* **2008**, *455*, 497−502.
(11) Tate, C. G.; Schertler, G. F. *Curr. Opin. Struct. Biol.* **2009**, *19*, 386−395.
(12) Rasmussen, S. G. F.; DeVree, B. T.; Zou, Y.; Kruse, A. C.; Chung, K. Y.; Kobilka, T. S.; Thian, F. S.; Chae, P. S.; Pardon, E.; Calinski, D.; Mathiesen, J. M.; Shah, S. T. A.; Lyons, J. A.; Caffrey, M.; Gellman, S. H.; Steyaert, J.; Skiniotis, G.; Weis, W. I.; Sunahara, R. K.; Kobilka, B. K. *Nature* **2011**, *477*, 549−55.
(13) Rasmussen, S. G. F.; Choi, H.-J.; Fung, J. J.; Pardon, E.; Casarosa, P.; Chae, P. S.; Devree, B. T.; Rosenbaum, D. M.; Thian, F. S.; Kobilka, T. S.; Schnapp, A.; Konetzki, I.; Sunahara, R. K.; Gellman, S. H.; Pautsch, A.; Steyaert, J.; Weis, W. I.; Kobilka, B. K. *Nature* **2011**, *469*, 175−80.
(14) Wright, P. E.; Dyson, H. J. *J. Mol. Biol.* **1999**, *293*, 321−31.
(15) Papermaster, D. S. *Methods Enzymol.* **1982**, *81*, 48−52.
(16) Kisselev, O. G.; Downs, M. A. *Biochemistry* **2006**, *45*, 9386−92.
(17) Elgeti, M.; Kazmin, R.; Heck, M.; Morizumi, T.; Ritter, E.; Scheerer, P.; Ernst, O. P.; Siebert, F.; Hofmann, K. P.; Bartl, F. J. *J. Am. Chem. Soc.* **2011**, *133*, 7159−65.
(18) Elgeti, M.; Ritter, E.; Bartl, F. J. *Z. Phys. Chem.* **2008**, *222*, 1117−1129.
(19) Vogel, R.; Siebert, F. *J. Biol. Chem.* **2001**, *276*, 38487−93.
(20) Mahalingam, M.; Martínez-Mayorga, K.; Brown, M. F.; Vogel, R. *Proc. Natl. Acad. Sci. U.S.A.* **2008**, *105*, 17795−800.
(21) Ye, S.; Zaitseva, E.; Caltabiano, G.; Schertler, G. F. X.; Sakmar, T. P.; Deupi, X.; Vogel, R. *Nature* **2010**, *464*, 1386−9.

(22) Zaitseva, E.; Brown, M. F.; Vogel, R. *J. Am. Chem. Soc.* **2010**, *132*, 4815−21.
(23) Fahmy, K.; Jäger, F.; Beck, M.; Zvyaga, T. A.; Sakmar, T. P.; Siebert, F. *Proc. Natl. Acad. Sci. U.S.A.* **1993**, *90*, 10206.
(24) Kisselev, O. G.; Meyer, C. K.; Heck, M.; Ernst, O. P.; Hofmann, K. P. *Proc. Natl. Acad. Sci. U.S.A.* **1999**, *96*, 4898−4903.
(25) Nishimura, S.; Kandori, H.; Maeda, A. *Biochemistry* **1998**, *37*, 15816−24.
(26) Bartl, F. J.; Ritter, E.; Hofmann, K. P. *FEBS Lett.* **2000**, *473*, 259−64.
(27) Vogel, R.; Martell, S.; Mahalingam, M.; Engelhard, M.; Siebert, F. *J. Mol. Biol.* **2007**, *366*, 1580−8.
(28) Choe, H.-W.; Kim, Y. J.; Park, J. H.; Morizumi, T.; Pai, E. F.; Krauss, N.; Hofmann, K. P.; Scheerer, P.; Ernst, O. P. *Nature* **2011**, *471*, 651−5.
(29) Barth, A. *Biochim. Biophys. Acta* **2007**, *1767*, 1073−101.
(30) Goormaghtigh, E.; Cabiaux, V.; Ruysschaert, J. M. *Subcell. Biochem.* **1994**, *23*, 405−50.
(31) Provasi, D.; Filizola, M. *Biophys. J.* **2010**, *98*, 2347−55.
(32) Okada, T.; Sugihara, M.; Bondar, A.-N.; Elstner, M.; Entel, P.; Buss, V. *J. Mol. Biol.* **2004**, *342*, 571−83.
(33) Frauenfelder, H.; Sligar, S.; Wolynes, P. *Science* **1991**, *254*, 1598−1603.
(34) Frauenfelder, H.; Chen, G.; Berendzen, J.; Fenimore, P. W.; Jansson, H.; McMahon, B. H.; Stroe, I. R.; Swenson, J.; Young, R. D. *Proc. Natl. Acad. Sci. U.S.A.* **2009**, *106*, 5129−34.
(35) Henzler-Wildman, K.; Kern, D. *Nature* **2007**, *450*, 964−72.
(36) Okada, T.; Ernst, O. P.; Palczewski, K.; Hofmann, K. P. *Trends Biochem. Sci.* **2001**, *26*, 318−24.
(37) Knierim, B.; Hofmann, K. P.; Ernst, O. P.; Hubbell, W. L. *Proc. Natl. Acad. Sci. U.S.A.* **2007**, *104*, 20290−5.
(38) Robinson, P. R.; Cohen, G. B.; Zhukovsky, E. A.; Oprian, D. D. *Neuron* **1992**, *9*, 719−25.
(39) Kisselev, O. G.; Kao, J.; Ponder, J. W.; Fann, Y. C.; Gautam, N.; Marshall, G. R. *Proc. Natl. Acad. Sci. U.S.A.* **1998**, *95*, 4270.
(40) Park, J. H.; Scheerer, P.; Hofmann, K. P.; Choe, H.-W.; Ernst, O. P. *Nature* **2008**, *454*, 183−7.
(41) Altenbach, C.; Yang, K.; Farrens, D. L.; Farahbakhsh, Z. T.; Khorana, H. G.; Hubbell, W. L. *Biochemistry* **1996**, *35*, 12470−8.
(42) Jaakola, V.-P.; Prilusky, J.; Sussman, J. L.; Goldman, A. *Protein Eng., Des Sel.* **2005**, *18*, 103−10.
(43) Lambright, D. G.; Sondek, J.; Bohm, A.; Skiba, N. P.; Hamm, H. E.; Sigler, P. B. *Nature* **1996**, *379*, 311−9.
(44) Ubbink, M. *FEBS Lett.* **2009**, *583*, 1060−6.
(45) Orban, T.; Jastrzebska, B.; Gupta, S.; Wang, B.; Miyagi, M.; Chance, M. R.; Palczewski, K. *Structure* **2012**, *20*, 826−40.
(46) Csermely, P.; Palotai, R.; Nussinov, R. *Trends Biochem. Sci.* **2010**, *35*, 539−46.
(47) Ma, B.; Kumar, S.; Tsai, C.-J.; Nussinov, R. *Protein Eng.* **1999**, *12*, 713−20.
(48) Herrmann, R.; Heck, M.; Henklein, P.; Henklein, P.; Kleuss, C.; Hofmann, K. P.; Ernst, O. P. *J. Biol. Chem.* **2004**, *279*, 24283−90.
(49) Lehmann, N.; Alexiev, U.; Fahmy, K. *J. Mol. Biol.* **2007**, *366*, 1129−41.
(50) Fritze, O.; Filipek, S.; Kuksa, V.; Palczewski, K.; Hofmann, K. P.; Ernst, O. P. *Proc. Natl. Acad. Sci. U.S.A.* **2003**, *100*, 2290−5.
(51) Ernst, O. P.; Gramse, V.; Kolbe, M.; Hofmann, K. P.; Heck, M. *Proc. Natl. Acad. Sci. U.S.A.* **2007**, *104*, 10859−64.
(52) Whorton, M. R.; Bokoch, M. P.; Rasmussen, S. G. F.; Huang, B.; Zare, R. N.; Kobilka, B.; Sunahara, R. K. *Proc. Natl. Acad. Sci. U.S.A.* **2007**, *104*, 7682−7.
(53) Jastrzebska, B.; Ringler, P.; Lodowski, D. T.; Moiseenkova-Bell, V.; Golczak, M.; Müller, S. A.; Palczewski, K.; Engel, A. *J. Struct. Biol.* **2011**, *176*, 387−94.
(54) Heck, M.; Hofmann, K. P. *J. Biol. Chem.* **2001**, *276*, 10000−9.
(55) Scheerer, P.; Heck, M.; Goede, A.; Park, J. H.; Choe, H.-W.; Ernst, O. P.; Hofmann, K. P.; Hildebrand, P. W. *Proc. Natl. Acad. Sci. U.S.A.* **2009**, *106*, 10660−10665.
(56) Shoemaker, B. A.; Portman, J. J.; Wolynes, P. G. *Proc. Natl. Acad. Sci. U.S.A.* **2000**, *97*, 8868−73.
(57) Chung, K. Y.; Rasmussen, S. G. F.; Liu, T.; Li, S.; DeVree, B. T.; Chae, P. S.; Calinski, D.; Kobilka, B. K.; Woods, V. L.; Sunahara, R. K. *Nature* **2011**, *477*, 611−5.
(58) Preininger, A. M.; Meiler, J.; Hamm, H. E. *J. Mol. Biol.* **2013**, *425*, 2288−98.